A scalable and cost-effective zinc-based MOF for efficient Cu(II) and Pb(II) removal from aqueous solutions

*Jinfeng Zhang†, Yuxin Liu†, Shuo Lin‡, Guilherme H. F. Melo†, George K. H. Shimizu‡, Uttandaraman Sundararaj†**

†Department of Chemical and Petroleum Engineering, University of Calgary, AB T2N 1N4 Canada

‡Department of Chemistry, University of Calgary, AB T2N 1N4 Canada

Keywords: Metal-organic framework, CALF-20, cost-effective, adsorbent, Cu(II) and Pb(II) removal

Abstract: The development of metal-organic frameworks (MOFs) for heavy metals removal from water faces ongoing challenge related to balancing performance with cost-effective synthesis. In this work, we report the first application of Calgary Framework 20 (CALF-20), a zinc-based MOF synthesized via a low-cost method, for the efficient adsorption of Cu(II) and Pb(II) ions from aqueous solutions. Synthesized at room temperature using commercially available, inexpensive reagents and green solvents, CALF-20 represents a highly economical alternative to many conventional MOFs. It exhibited excellent adsorption efficiency, achieving uptake

capacities of 250 mg/g for Cu(II) and 833 mg/g for Pb(II) at the optimum pH of 5.3, outperforming many MOFs reported to date. Adsorption kinetics followed the pseudo-second-order model, while equilibrium data aligned well with the Langmuir isotherm. CALF-20 was demonstrated strong performance under competitive ion conditions, removing over 99% of Cu(II) and 80% of Pb(II). The material's high adsorption capacity, low synthesis cost, chemical robustness, and reusability across multiple cycles underscore its potential for industrial scale water treatment and environmental remediation.

1. INTRODUCTION

The impact of heavy metals like copper (Cu) and lead (Pb) pollution of water sources has far reaching environmental and health consequences because of their non-biodegradability, high toxic, and bioaccumulation in aquatic ecosystems.[1-2] Expose and excessive intake of these metals can lead to several types of metabolic and physiological disorders in humans, animals, and plants.[2-3] The source of these metals can be attributed to different industries, mineral processing, metal plating and battery manufacturing among others[4], making the efficient removal strategies of these metal ions a critical global challenge.

Several treatment methods have been used to remove heavy metal ions from aqueous media, including evaporation, electrodeposition, chemical precipitation, membrane separation, and ion exchange, however, they are often suffering from high operational costs, incomplete ion removal, ineffective, and harmful to the environment.[5-6] Adsorption-based technologies are widely recognized and considered as a popular choice alternative to aforementioned methods for their cost-effectiveness, flexibility in design, operational simplicity, reversibility, and high removal efficiency.[7] The efficiency of adsorption method is largely constrained by the ability to design adsorbents with the necessary physical and chemical functionalities tailored for the target contaminant. Porous materials such as metal-organic frameworks (MOFs)[8-9] have been shown to be very effective adsorbents[10-11] for heavy metal ions because of their high surface area, tunable pore size, and numerous number of active sites. MOFs are advanced inorganic-organic hybrid materials[12] that allow for the systematic buildup of metal clusters and organic linkers into topologically well-defined porous architectures. Reticular chemistry[13-17] has been developed as a discipline over the last decade and topology diagrams and synthetic methodologies are now available to create a vast number of MOFs with potential applications. Recent developments

have led to the synthesis of numerous MOFs with high selectivity and affinity towards the target pollutants, Cu(II) and/or Pb(II), based on variation in surface area, pore size, and chemistry for the environmental remediation.[10, 18] MOF-5, a cubic MOF compound synthesized from zinc and 1,4-terephthalic acid, showed a maximum uptake of 289.9 mg/g on Cu(II) and 517.6 mg/g on Pb(II) at a pH of 5.2.[19] Upon changing the zinc to copper, Rahimi and Mohaghegh found that the copper-terephthalate MOF, Cu(tpa)(dmf), only showed an uptake of Cu(II) and Pb(II) with 71.9 mg/g and 35.1 mg/g at a pH of 7, respectively.[20] Shooto et al. reported a Cadmium-based MOF, which is non-porous to N_2, exhibiting a 183.4 mg/g uptake of Cu(II) and 171.4 mg/g removal of Pb(II) from aqueous solutions without cadmium ion leaching.[21] Ghaedi et al. also used a Cadmium-based MOF, MOF-2(Cd), for the removal of Cu(II) and Pb(II) in aqueous solutions. They found that the MOF-2(Cd) was not only chemical and thermal stable but also had a maximum monolayer adsorption capacity of 434.8 and 769.2 mg/g, respectively, towards Cu(II) and Pb(II) at a pH 6 aqueous solution.[22] Other MOF materials, such as ZIF-8[23], UiO-66[24-26], Cd-MOF-74[27], etc., were also investigated for their potential use in Cu(II) and/or Pb(II) ions removal. Despite extensive research on MOFs for wastewater treatment, many exhibit significant limitations, including low sensitivity for target ions, insufficient adsorption capacity, and vulnerability to humidity and acidity due to the hydrolysis of metal ligand bonds.[28] Additionally, their synthesis methods are often not optimized for cost-effective large-scale heavy metal ion removal, making practical application challenging.[29] Therefore, developing selective adsorbent with high adsorption capacity, rapid kinetics, and cost-effective is crucial for advancing wastewater treatment technologies.

Zinc-based Calgary Framework 20 (CALF-20) is a MOF that has recently demonstrated for selective separations due to the high chemical robustness and precise structural design[30]. Notable

is that while many other MOFs are unstable in humid conditions, and are thus not suitable for use in steam or wet acid gases environments, CALF-20 is stable and performs well in such conditions, which makes it suitable for real life use.[30-31] The structure of this zinc-based MOF reveals a 3D nanoscale lattice with high pore interconnection, a feature that would suggest suitability for adsorption of heavy metal ions. Lin et al.[30] documented that a high product yields of up to 90% and an exceptional space-time yield of 550 kg/m^3 day can be achieved by using methanol and water as solvents, as well as low cost, commercially available starting materials. In 2023, BASF in collaboration with Canadian company Svante had successfully scaled up CALF-20 from lab-scale to industrial scale with an estimation of more than 200 tons per year[32] by using a simple low-temperature process in accordance with green chemistry principles. With the hundred-ton scale production, the price of CALF-20 is estimated to be $20-30 per kg[32-33].

Here, for the first time, we report the heavy metal adsorption performance of CALF-20 in both batch and continuous flow systems, focusing on its applicability for Cu(II) and Pb(II) removal (Scheme 1). Coupled aqueous coordination chemistry and supramolecular assembly, a simple, green, and scalable synthesis approach of CALF-20 at ambient temperature and pressure was achieved. The effective of pH, initial concentration, contact time, and coexisting cations on the adsorption process were evaluated. As-synthesized CALF-20 demonstrated significant Cu(II) and Pb(II) capture capabilities compared to its MOF analogues, due to its microporous structure, stable framework, and high surface area. The adsorption isotherms, kinetics, reusability, and adsorption mechanism were analyzed and investigated. With this comprehensive evaluation of CALF-20's feasibility in Cu(II) and Pb(II) removal, this work aims to demonstrate its potential for wastewater remediation applications.

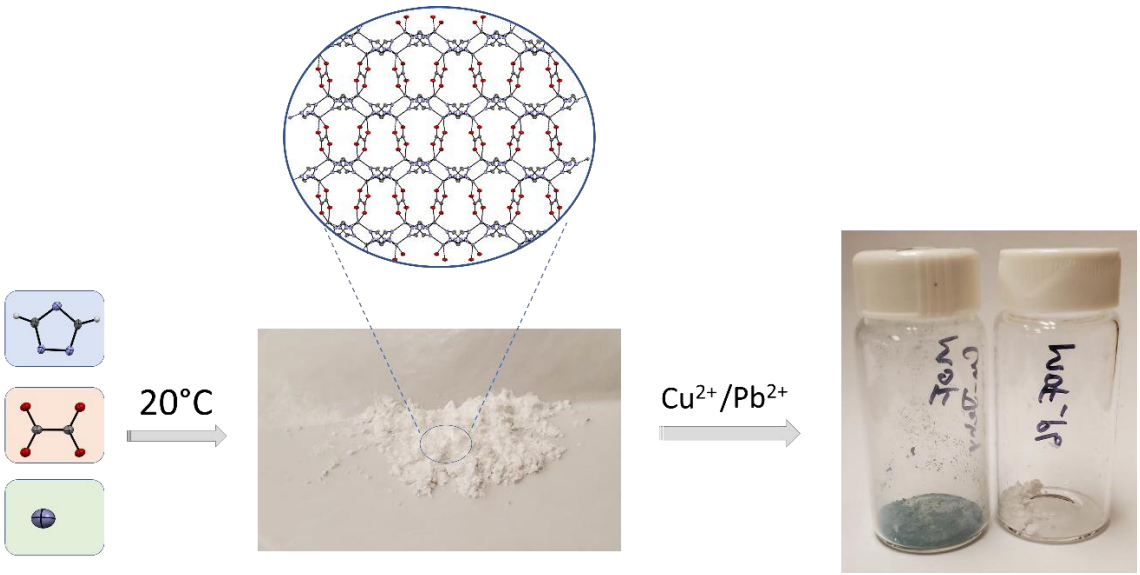

Scheme 1 Schematic illustration of room temperature synthesis of CALF-20 for Cu(II) or Pb(II) capture.

2. MATERIALS AND METHODS

2.1 Chemical reagents

1*H*-1,2,4-triazole (≥98%, Sigma-Aldrich), argon (Ar, 99.999%, Air Liquide), carbon dioxide (CO_2, 99.999%, Air Liquide), copper(II) nitrate trihydrate (≥99.5%, Sigma-Aldrich), hydrochloric acid (HCl, 36.5 to 38.0%, Fisher), methanol (≥99.8%, Fisher), nitric acid (HNO_3, 70%, Fisher), nitrogen (N_2, 99.999%, Air Liquide), lead(II) nitrate (≥99.0%, Sigma-Aldrich), sodium hydroxide (NaOH, ≥97%, Sigma-Aldrich), sodium oxalate (≥99.5%, Sigma-Aldrich), thiourea (≥99%, Sigma-Aldrich), and zinc acetate dihydrate (>98%, Sigma-Aldrich) were used without further purification.

2.2 Synthesis procedures

The synthesis of CALF-20 powder was carried out based on the method reported in the literature with modification.[34] In a 150 mL water/methanol solution (120/30, v/v), 5.50g, 0.025 mol of $Zn(OAc)_2$ $2H_2O$ was charged and stirred for 10 minutes to yield a clear solution. 1.675 g, 0.0125

mol of sodium oxalate was then added to previous solution to form a suspension and stirred for another 10 minutes. 3.45 g, 0.05 mol of 1*H*-1,2,4-triazole was then added to the suspension, and the mixture was stirred for 60 minutes to generate CALF-20 particles. Once done, the precipitate was isolated via centrifugation, washed several times with RO water, and dried at 130°C under vacuum overnight for further use. An 83% yield based on the mass of Zn source was achieved.

2.3 Characterizations

The structure of CALF-20 was characterized using an X-ray diffractometer (XRD, D8 Advance (ECO), Bruker AXS, Germany) equipped with a Copper-source X-ray (1.5406 Å) within a 2θ angle of 5 to 45°. Fourier transform infrared spectroscopy (FTIR) data were collected in the wavenumbers ranging from 4000 to 400 cm^{-1} on a Fourier-transform infrared spectrometer (Agilent Cary 630, Agilent Technologies Inc., USA). The concentration of heavy metallic ions was determined using an inductively coupled plasma optical emission spectrometer (ICP-OES, iCAP 7200, Thermo Scientific, USA). Gas sorption analyses were conducted via a Micromeriticis ASAP 2460 or a TriStar II Surface Area and Porosity Analyzer (Micromeritics Instrument Corporation, USA). The structural morphology and elemental content distribution were probed on a FEI XL30 scanning electron microscopy (SEM-EDS) instrument (Philips, USA). The zeta potential measurements of CALF-20 were carried out using a Zetasizer Nano ZS (Malvern Panalytical, UK). X-ray photoelectron spectrometry (XPS) was carried out using an ESCALAB QXi (Thermo Scientific, USA) and the analysis was conducted on a K-Alpha plus X-ray photoelectron spectrometer using Al-Kα as the excitation source.

2.4 Batch heavy metal ion adsorption experiments

The adsorption experiments were carried out based on single-factor effects. The effect of concentration ([Cu^{2+}]=1-400 mg/L, [Pb^{2+}]=1-600 mg/L), time (0 to 480 min), pH (3 to 9), and removal efficiency on the adsorption of Cu(II) and Pb(II) were studied in a batch method. Briefly, 2.5 mg of the CALF-20 adsorbent was dispersed to 10 mL of aqueous solutions, which were prepared by dissolving copper(II) nitrate and lead(II) nitrate in reverse osmosis (RO) water at room temperature. The pH values were adjusted with diluted HCl and NaOH solutions, the mixture was shaken at 20 °C for 360 min. After extraction, the metal ion concentrations were monitored by ICP-OES. The adsorption capacity (q_t, mg/g) and removal efficiency (R%) were calculated using Equation (1) and Equation (2), respectively.

$$q_t = (C_0 - C_e) \times V/W \qquad (1)$$

$$R = (1 - C_0/C_e) \times 100\% \qquad (2)$$

Where C_0 (mg/L) and C_e (mg/L) are the initial and equilibrium concentrations for metal ions, respectively, V (L) refers to the volume of the solution, and W (g) refers to the mass of the adsorbent.

Desorption studies were conducted to examine the repeated regeneration of CALF-20. In these experiments, the adsorbed CALF-20 was washed with a 0.3 M thiourea solution containing 0.001 M HCl after adsorbing Cu(II) and Pb(II). Specifically, 160 mg of CALF-20 was dispersed in 40 mL of Cu(II) solution (~400 mg/L, pH 5.3) and shaken at 20°C for 4 hours. Following centrifugation, the used CALF-20 was added to 15 mL of thiourea solution and shaking was done for another 60 minutes. After separating the solid from the liquid, another portion of 15 mL of thiourea solution was added to the solid for an additional 60 minutes. Once this process was complete, the solid was separated using a centrifuge, and the regenerated CALF-20 was washed

several times with RO water until it reached a neutral pH. The regenerated CALF-20 was then vacuum-dried and reintroduced into a fresh Cu(II) or Pb(II) solution and shaken for 4 hours to assess its adsorption capacity. The regeneration efficiency was calculated based on the amount of metal ions adsorbed and desorbed using ICP-OES. These adsorption-desorption cycles were repeated five times.

2.5 Multi-component batch adsorption experiments.

Multi-component batch adsorption experiments were conducted to evaluate the performance of CALF-20 in removing Cu(II) and Pb(II) ions simultaneously. A solution containing varying concentrations (0.07-5.30 ppm) of multiple heavy metal ions (Cu(II), Pb(II), Ni(II), Cr(III), and Fe(III)) was prepared to simulate the composition of a coal mine waste water[35]. Different dosage of CALF-20 sample (0.25, 0.5, 1.0, and 2.0 g/L) was added to a beaker containing 40 ml of mixed ion solution. The mixture was maintained at room temperature for 4 hours with stirring before filtering through a 0.45 μm syringe filter. The filtrates were subsequently analyzed using ICP-OES to determine the concentration of residual metal content.

2.6 Fixed-bed dynamic breakthrough experiment

CALF-20 sample (approximately 5.0 g) was packed into a column with an inner diameter of approximately 20 mm and a packed length of about 3 cm. An aqueous solution containing both heavy metal ions (Cu(II) and Pb(II)) at a concentrations of about 5 ppm passed through the column at a flow rate of 1.5 mL/min at room temperature. The filtrates were subsequently analyzed using ICP-OES to determine the concentration of the residual metal content.

3. RESULTS AND DISCUSSION

3.1 Characterization

The structure of CALF-20 was reported and discussed in the paper published in 2021 by the George Shimizu group[30] and frameworks built from Zn(II), triazolate (trz) and oxalate (ox) ions were published and discussed earlier [36-38]. CALF-20 is composed of layers of 1,2,4-triazole-bridged zinc(II) ions pillared by oxalate ions to form a three-dimensional lattice and three-dimentional pore structure, as illustrated in Figure 1a-c. The synthesized CALF-20 was confirmed using X-ray diffraction (XRD) in the range of $2\theta = 5°–45°$ with the black simulated pattern reported in literature[39], as shown in Figure 1d. The main characteristic peaks for the as-synthesized CALF-20 are consistent with the simulated CALF-20 pattern indicating a successful synthesis. The CALF-20 powders acquired prior to, and post adsorption process were examined to study the change in crystalline features of the adsorbent. The existence of sharp and intense XRD peaks in these samples indicates a high degree of crystallinity. The major peaks in the PXRD of CALF-20 are retained after metal sorption and desorption.

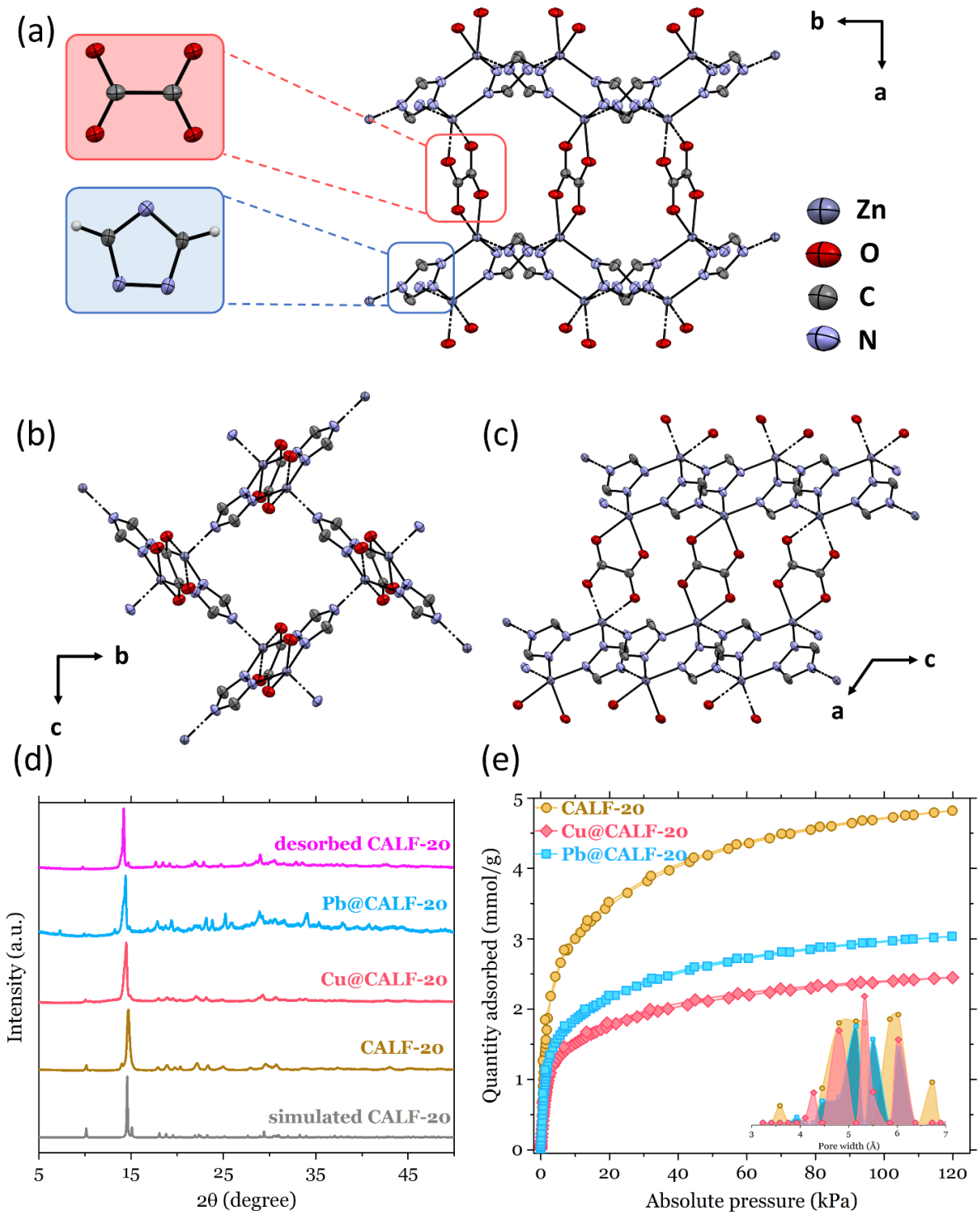

Figure 1 (a) View of ab plane of crystal structure of CALF-20 showing the pillaring of the zinc triazolate corrugated layers by oxalate anions; (b) view of b-axis of CALF-20 showing the 2-D layer constructed by zinc(II) and triazole ligands; (c) view of b-axis of CALF-20 showing the zinc coordination spheres; (d) PXRD patterns of CALF-20 simulated, CALF-20, Cu@CALF-20, Pb@CALF-20, and CALF-20 after desorption; (e), 273K CO_2 isotherm of CALF-20, Cu@CALF-20, and Pb@CALF-20 (Inserted pore size distribution calculated by the NLDFT method). All hydrogens are omitted in crystal structures for clarity.

193 The acquired N_2 adsorption/desorption isotherms at 77K for CALF-20, Cu@CALF-20, and
194 Pb@CALF-20 are presented in Figure S1. It can be observed that at low relative pressures (P/P_0),
195 there is a rapid increase in N_2 adsorption, followed by a plateau-like behavior. The isotherm
196 bends towards the P/P_0 axis and then exhibits a plateau, with the adsorption reaching a saturation
197 point. These characteristics typify a Type I isotherm distribution based on the IUPAC
198 (International Union of Pure and Applied Chemistry) classification.[40] The pronounced increase
199 observed at low pressures is predominantly due to enhanced interaction between the adsorbent
200 and adsorbate within the micropores, causing these pores to fill at remarkably low pressures. The
201 curve rises again when approaching saturation pressure ($P/P_0 > 0.8$), mainly due to condensation
202 of the adsorbate. These isotherms also indicate that the primary pores of CALF-20, Cu@CALF-
203 20 and Pb@CALF-20 are mainly micropores. CALF-20 demonstrated a BET surface area of 500
204 m^2/g (Table S1), consistent with previously reported literature values[30], confirming the successful
205 synthesis of the material. Notably, this surface area is significantly higher compared to
206 Cu@CALF-20 (328 m^2/g) and Pb@CALF-20 (200 m^2/g).

207 The porosity of CALF-20 was also evaluated by CO_2 isotherm at 273 K since CALF-20 is
208 renowned for precise pore design on CO_2 capture. Isotherms were collected for CALF-20,
209 Cu@CALF-20, and Pb@CALF-20, and are depicted in Figure 1b. All three samples give Type I
210 isotherm according to IUPAC classification[40] indicating the exist of pore size distributions over a
211 broader range including wider micropores and possibly narrow mesopores (less than 2.5 nm),
212 which agrees with the N_2 isotherm results. At 120 kPa, the CO_2 capacities are 4.82, 3.03, and
213 2.45 mmol/g for CALF-20, Cu@CALF-20, and Pb@CALF-20, respectively. The isotherms of
214 CALF-20 post Cu(II) and Pb(II) adsorption reach their 'knee' earlier than CALF-20 indicating
215 they have less available surface area. All three samples adsorb a considerable amount of CO_2 in

the low-pressure region, however, there is a significant difference between their total CO_2 uptakes. When metal ions were loaded, a 40%-50% uptake capacity decrease was observed.

To better probe the change of the characteristics of CALF-20 post metal ion adsorption, the pore size distribution of all three samples were also calculated using a NLDFT method[41] on their 273K CO_2 isotherm data. As inserted picture shown in Figure 1e, CALF-20 has micropores with a diameter of 3.6, 5.0, 6.0, 6.8, and 8.0 Å. When metal ions were introduced, these narrowest pores were likely occupied by metal ions as indicated by the decreased incremental pore volume for all pore size ranges.

The CALF-20 sample was characterized by SEM to investigate the surface morphology (Figure S2). The crystals of the original CALF-20 sample are irregular polyhedrons with a smooth surface and have an average size of 300-400 nm width and 400-500 nm length.

The cost for manufacturing of CALF-20 was calculated using the method reported by Ashley Sutton[42] based on the raw materials used. Although different starting materials employed, a same USD $29 per kg manufacture cost was achieved and the break down calculation can be found in Table S2.

3.2 Batch adsorption studies

The pH of the solution has an impact on the surface charge density and adsorption capacity of the adsorbent during the actual adsorption process. To investigate the effect of pH on the adsorption efficiency of Cu(II) and Pb(II) by CALF-20, we analyzed the zeta potential of CALF-20 across different pH values (Figure S3). As shown in Figure S3, CALF-20 carried positive charges at pH 2-7. Figure S4 summarized the adsorption capacity of CALF-20 on Cu(II) and Pb(II) at different

pH environments and the default pH of the Cu(II) and Pb(II) solution was 5.3. The maximum adsorption capacity for Cu(II) and Pb(II) at 100 ppm were 350 mg/g at pH 4.5 and 504 mg/g at pH 5.3, respectively. At low pH values (<4), metal ions were competed with large amount of H_3O^+ for the active sites on the adsorbent surface.[43] When pH was higher than 4.5 for Cu(II) and 5.3 for Pb(II), the adsorption capacity of CALF-20 for both ions decreased, due to the lesser amount of reactive groups on the adsorbent surface. On the other hand, for a neutral or basic environment, metal hydroxide precipitates out for both ions[44], lowering the adsorption capacity. Given so, pH 5.3 was used for further adsorption studies of CALF-20 on Cu(II) and Pb(II).

The effect of contact time on the adsorption properties of CALF-20 for Cu(II) and Pb(II) ions was investigated in a solution with a pH of 5.3 at 20°C. As shown in Figure 2a, the adsorption of both Cu(II) and Pb(II) by CALF-20 is rapid during the first 20 minutes. This initial fast adsorption is primarily due to the abundance of accessible active sites on the surface of CALF-20 and the significant concentration gradient between the bulk solution and the solid-liquid interface, which provides a strong driving force for adsorption. After 20 minutes, a large number of Cu(II) and Pb(II) ions occupy the adsorption sites on the surface and within the structural voids of CALF-20, slowing the adsorption rate. At this stage, new metal ions must diffuse through the pore channels of CALF-20 to access the less accessible internal adsorption sites, resulting in a slower adsorption rate until equilibrium is reached. For Cu(II), adsorption equilibrium is achieved at around 15 minutes, with an adsorption capacity of 225 mg/g reached. The uptake of Pb(II), on the other hand, shows a slower uptake rate and equilibrium is reached only at about 240 minutes.

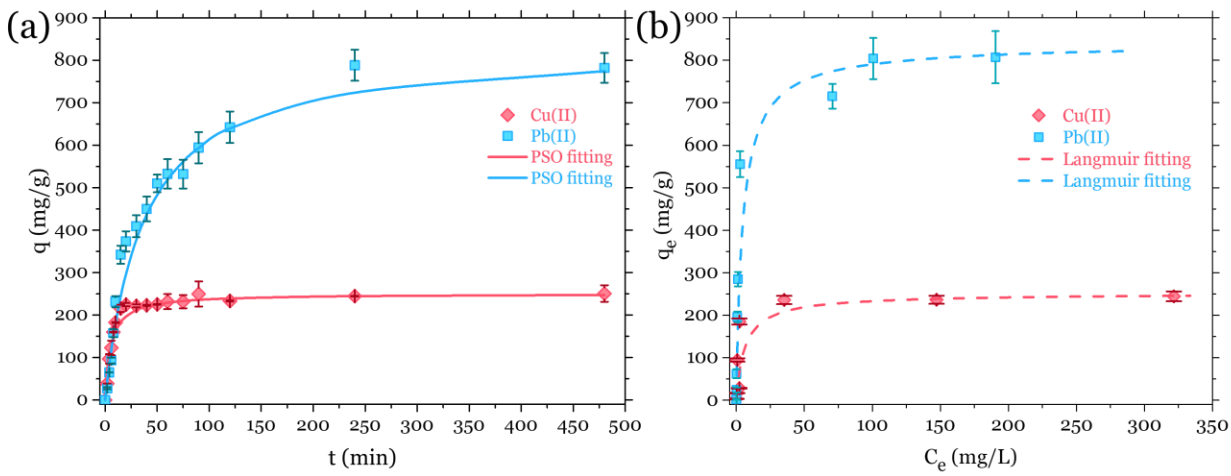

Figure 2 Adsorption kinetics (a) and isotherms (b) of Cu(II) and Pb(II) uptake by CALF-20. During the experiment, 10 mg of CALF-20 was exposed to a Cu(II) and Pb(II) solution at pH 5.3.

The kinetic properties of CALF-20 adsorption of both Cu(II) and Pb(II) were investigated by pseudo-first-order (PFO) model,[45] pseudo-second-order (PSO) model,[46] Elovich model,[47] and Weber-Morris intra-particle diffusion[48] kinetic model, as listed in Table S4. Based on the data presented in Table 1 and the regression analysis in Figure 2b, Figure S5, and Figure S8, the correlation coefficients (R^2) and calculated q_e values indicate that the pseudo-second-order (PSO) kinetic model provides the most accurate fit of the adsorption kinetics of Cu(II) and Pb(II) onto CALF-20, surpassing other kinetic models.

Table 1 Kinetic model data of Cu(II) and Pb(II) adsorption by CALF-20.

Parameters	Metal ions	
Experimental	Cu(II)	Pb(II)
$q_{e(exp)}$ (mg/g)	250	788
Pseudo-first order		
q_e (mg/g)	60.1	579
k_1 (1/ min)	0.01	0.0098
R^2	0.5884	0.9676
Pseudo-second order		
q_e (mg/g)	250	833
k_2 (g/(mg min))	0.00073	0.000033
R^2	0.9995	0.9926
Elovich		
α	303	70.2
β	0.028	0.0063
R^2	0.7653	0.9780
Weber-Morris Intra-particle diffusion		
K_{p1}	59.9	79.1
C_1	-18.0	-42.8
R^2	0.9626	0.9494
K_{p2}	1.86	19.4
C_2	215	405
R^2	0.7090	0.8216

To further identify the rate-controlling steps during the adsorption mechanism, the Weber-Morries intra-particle diffusion model was applied.[49-50] As illustrated in Figure S6 and S9, the Weber-Morris plot of q_e vs. $t^{1/2}$ reveals two distinct stages with different line slopes. Since these slop lines do not pass through the origin point(C1≠0 in Table 1), the intra-particle diffusion is not the only rate-controlling step in a complex mechanism and the adsorption process involves both external and internal diffusion. Specifically, the first stage relates to instantaneous adsorption or external surface adsorption, characterized by its high slope values (K_{p1}), indicating a rapid uptake rate of Cu(II) and Pb(II) ions at the beginning of the adsorption process. This is due to the abundance of active sites on the adsorbent surface. The second stage, which represents progressive adsorption or intra-particle diffusion, has lower slopes (K_{p2}) reflecting a reduced concentration gradient of the adsorbates. This reflects a lower uptake rates given slower diffusion of Cu(II) and Pb(II) ions into the micropores of the adsorbent. Micropores in CALF-20 facilitates

effective mass transfer, minimizing the distance for copper and lead ions to migrate into the adsorbent, thereby enhancing diffusion efficiency and promoting adsorption. These findings suggest that intra-particle diffusion is indeed the primary rate-controlling process in the adsorption mechanism.

To understand more about the adsorption mechanism and investigate the interaction between adsorbent and adsorbate, the effect of the initial concentration of Cu(II) and Pb(II) on the adsorption capacity at 20°C was studied and the adsorption isotherms were carried out. Solutions with varying concentrations of Cu(II) and Pb(II) were prepared to evaluate the performance of the adsorbent. The adsorption isotherm of both Cu(II) and Pb(II) ions on the CALF-20 is presented in Figure 2b, with the equilibrium concentration (C_e) on the x-axis and the amount adsorbed at equilibrium (q_e) on the y-axis. CALF-20 has an equilibrium uptake of 250 and 788 mg/g for Cu(II) and Pb(II), respectively, which is higher than most reported MOF adsorbents (Table S5), highlighting its superior adsorption capacity.[10, 35, 51]

To better understand the effect of concentration on the nature of Cu(II) and Pb(II) adsorption by CALF-20, we examined the adsorption isotherms using the Langmuir,[52] Freundlich,[53] Langmuir-Freundlich,[54] Temkin,[55] and Dubinin-Radushkevich (D-R) models (Figure S7 and Figure S10, respectively). The corresponding isotherm equations are provided in Table S3. According to the correlation data presented in Table 2, the Langmuir isotherm exhibits the highest correlation coefficient (R^2) values, indicating it can fit the experimental data better than other models. The curve of experimental data follows a typical Langmuir isotherm, where q_e increases rapidly at low C_e values, indicating high adsorption efficiency. The maximum uptake capacities, q_m, derived from the Langmuir model are 250 mg/g for Cu(II) and 833 mg/g for Pb(II), closely matching the experimental values.

The removal efficiency of CALF-20 for Cu(II) and Pb(II) was compared across different metal ion concentration solutions. CALF-20 exhibited remarkable removal efficiency for Cu(II), achieving over 90% under all conditions and exceeding 95% for solutions with Cu(II) concentrations higher than 25 mg/L (Figure S11). For Pb(II), CALF-20 can remove about 90% at 1ppm Pb(II) solution and upon increase of concentration of Pb(II) ions in the aqueous solution, the removal efficiency increased to 96% - 98%. The high efficiency is likely due to CALF-20's extensive surface area, microporous structure, and strong binding affinity for metal ions, making it a promising candidate for industrial wastewater treatment and environmental remediation. These findings highlight the potential of CALF-20 in effectively removing heavy metal ions from contaminated water sources, with particularly high efficiency for Cu(II) and Pb(II).

Table 2 Parameters values for Cu(II) and Pb(II) adsorption obtained from different isotherm models.

Adsorbates	Cu(II)	Pb(II)
Langmuir		
q_m *(mg/g)*	250	833
K_L *(L/mg)*	0.179	0.240
R^2	0.9980	0.9977
Freundlich		
K_F *(L/mg)*	33.8	96.2
n	2.24	1.81
R^2	0.6980	0.7761
Dubinin-Radushkevich (D-R)		
β (mg/kJ)^2	8E-08	6E-08
E (kJ/mol)	2.50	2.89
R^2	0.6954	0.9101
Temkin		
K_T (L/mg)	13.4	18.8
b_t (J/mol)	77.9	24.3
R^2	0.7928	0.9464

To assess the metal ion removal performance, the uptake capacity of CALF-20 for Cu(II) and Pb(II) ions was compared with other MOF adsorbents reported in the literature in recent years, including ZIF-8, UiO-66, MIL-101, etc., and is listed in Table S5. Figure 3 shows that CALF-20 exhibits commendable uptake of Cu(II) ions and outstanding removal performance for Pb(II)

ions compared to other MOF adsorbents reported in the literature, demonstrating a stronger adsorption affinity and relatively high adsorption capacity for these heavy metals in aqueous solutions.

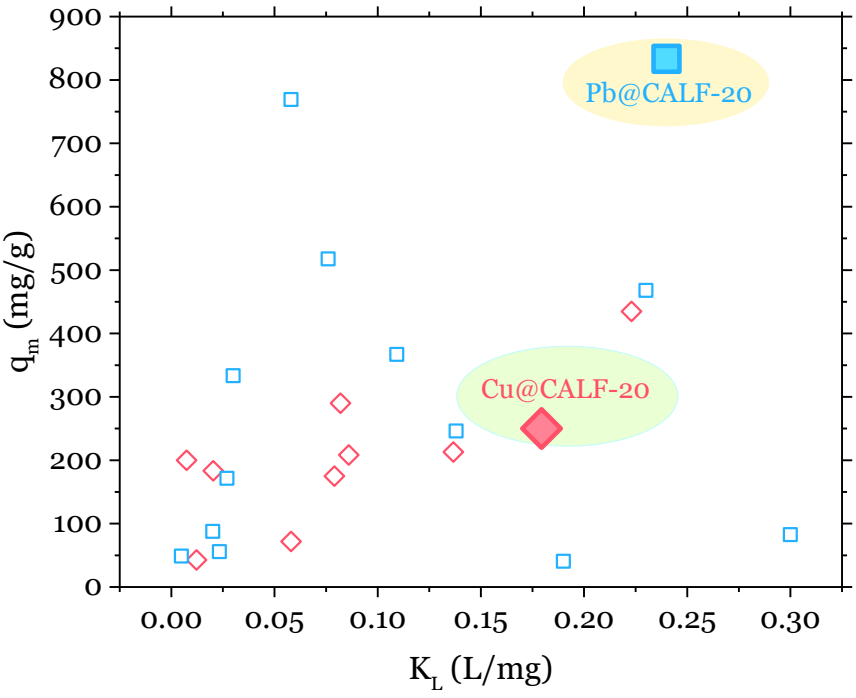

Figure 3 Performance of CALF-20 on Cu(II) or Pb(II) removal compared to reported MOF adsorbents.

3.3 Adsorption mechanism

To gain insight into the interaction of Cu(II) or Pb(II) with CALF-20, XPS spectra of pristine and metal-ion loaded CALF-20 were acquired in the binding energy regions of the Cu 2p, Pb 4f, N 1s, and O 1s orbitals (Figure S12). As shown in Figure 4a, pairs of Cu $2p_{1/2}$ and $2p_{3/2}$ doublets (at 953.3/933.5 and 954.8/935.3 eV) and the charge transfer shake-up satellites (at 963.4 and 944.2 eV) were observed on Cu@CALF-20, indicating the existence of Cu(I) and Cu(II), respectively, which agrees with literature[56]. For Pb@CALF-20, two peaks appear at 138.2 and 143.1 eV, attributed to Pb $4f_{7/2}$ and Pb $4f_{5/2}$, respectively[57], which can be associated with Pb-O bonding (Figure 4b). Additionally, two weaker peaks at 136.4 eV and 141.2 eV, corresponding to

Pb(0)[57], possibly due to free Pb(II) adsorbing onto CALF20 and being partly reduced to Pb(0). Figure 4c displays the N 1s spectrum of pristine CALF-20, Cu@CALF-20 and Pb@CALF-20, respectively, at 399 and 400.7 eV attributing to C-N and C=N bonds. Once metal ion is adsorbed, the spectrum of N 1s shifts towards lower binding energy, which indicates an electron density redistribution due to interaction between metal ion and the nitrogen atom.[58] Given that Cu(II) has a higher charge density compared to Pb(II), a more significant charge density redistribution and a larger shift in binding energy are observed. Similar trend is also observed from Figure 4d, which shows O 1s spectrum of pristine CALF-20, Cu@CALF-20 and Pb@CALF-20, respectively. Typically, the adsorption sites are depleted due to oxidation, resulting in a reduced adsorption capacity during subsequent reuse cycles. This represents a significant drawback for certain adsorbents, however, according to our XPS data, a substantial reduction of Cu(II) or Pb(II) was observed on the bidning energy of N 1s changes, possibly due to the metal-π interaction formed between the metal and the triazolate groups of CALF-20. The electron density transfer from the π-system of the triazolate ring to the copper ion facilitates the reduction of Cu(II) to Cu(I) and helps stabilize the Cu(I) state. With no N-O peak shows up on the N 1s spectra (Figure 4c),[59] it is likely that the Cu(II) or Pb(II) was reducted without oxidizing the aromatic amine on the CALF-20 framework and only through ligand-to-metal charge transfer[36-37, 60].

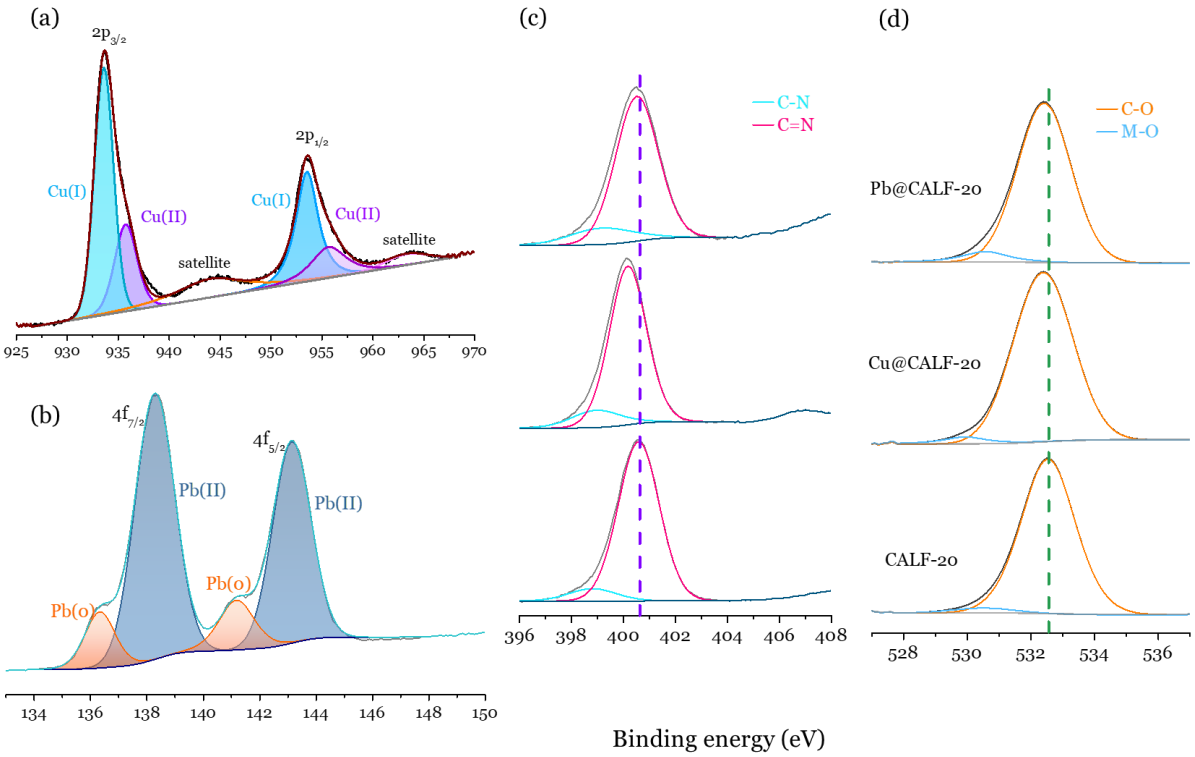

Figure 4 High resolution XPS spectra of (a) Cu 2p, (b) Pb 4f, and (c) N 1s and (d) O 1s of CALF-20, Cu@CALF-20, and Pb@CALF-20.

The XPS-detected reduction of metal ions during adsorption is also reported in the literature. In 2020, Jeffrey Urban and co-workers[56] published their work of a hydrogen-bonded organic-inorganic framework, zinc imidazole salicylaldoxime (ZIOS) for trace copper ion removal from water. The ZIOS was believed a better candidate than ZIF-8 and it was proved very stable in water. As their XPS results indicated, the copper(I) peaks showed in both ZIOS and ZIF-8 post adsorption. They believe this was caused by the change in coordination environment of Cu brought the electron donating/accepting ability changed. They also found the downshift of N 1s binding energy in ZIOS which is like our findings. Coincidentally, Xuwei Chen and co-workers[61] in their work of using a TbDa-COF for efficient and rapid extract Au(III) from e-waste solution also noticed the reduction of metal ions adsorbed. Their XPS spectra also indicated a reduction happened to Au(III) adsorbed and Au(0) characteristic peak was clearly observed. The shift of N

1s binding energy was also revealed and they believe the metal ion reduction was due to the electron donors supplied via TbDa-COF with electron rich N/O-containing groups in the capture process.

The CALF-20 samples prior and post metal ion adsorption were investigated by FTIR spectrometer and the FTIR spectra were plotted in Figure S13 in the range of 400-4000 cm^{-1}. The absorption peaks from CALF-20@Cu and CALF-20@Pb can be indexed to the ones on CALF-20, indicating the unchanged bond and structure of the adsorbent. Elemental mapping images of Cu(II) or Pb(II) loaded CALF-20 were obtained and shown in Figure S14. Cu(II) and Pb(II) are found to be evenly distributed in the mapping area, along with zinc and nitrogen maps, indicating that the adsorption predominantly happened on the surface.

3.4 Regeneration and reusability

To ensure cost-effectiveness and long-term feasibility in practical applications, solid sorbents are evaluated of their regenerative ability. Here, five adsorption-desorption cycles were applied to CALF-20 adsorbent and the desorption of the sorbent was conducted using an acidic thiourea solution. As shown in Figure 5, the adsorption capacity of CALF-20 towards Cu(II) and Pb(II) were retained even after five regeneration cycles. Specifically, CALF-20 exhibited an adsorption capacity of 95 mg/g and 80 mg/g for Cu(II) and Pb(II), respectively, at the first adsorption attempt. After five adsorption-desorption cycles, CALF-20 could retain an adsorption capacity of 93% for Cu(II) and 90% for Pb(II). This high regeneration efficiency highlights the structural robustness and chemical stability of CALF-20. These characteristics of CALF-20 also make it possible for industrial applications, and the ability to reuse adsorbents without significant loss in performance is crucial for controlling operation costs.

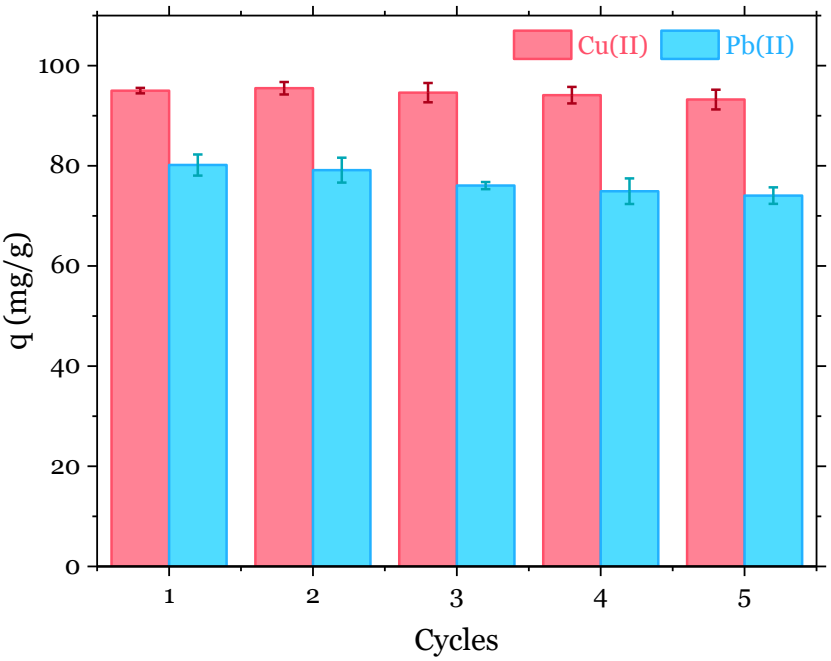

386

387 Figure 5 Reusability of CALF-20 adsorbent towards Cu(II) and Pb(II) in the adsorption-desorption
388 cycles.

389 3.5 Multi-ion adsorption

390 To assess the performance of CALF-20 for the removal of Cu(II) and Pb(II) in the presence of
391 competing cations, an aqueous solution containing five metal ions, including Cu(II), Pb(II),
392 Ni(II), Cr(III), and Fe(III), at varying concentrations ranging from 0.07 to 5.30 ppm, simulating
393 real coal mine wastewater[35], was utilized. The results, summarized in Table S6 and Figure 6,
394 demonstrate that with CALF-20 dosages ranging from 0.25 to 2 g/L, all metal ions can be
395 effectively removed simultaneously. Specifically, a removal rate exceeding 99% for Cu(II), 95%
396 for Cr(III), and 90% for Ni(II) was achieved. Conversely, the removal efficiency for Pb(II)
397 ranged between 75-82%. These outcomes are consistent with the single-component adsorption
398 test results, confirming CALF-20 is a desirable adsorbent for simultaneous removal of multiple
399 metal contaminants. This analysis can be extended further by considering the cost of the MOF
400 adsorbent associated with its performance. CALF-20 can be produced at USD $29 per kg[42] at the

kilogram scale and BASF has successfully scaled it to industrial scale[62] in 2023. The price-performance ratio of CALF-20 with a dosage of 0.25g/L, indicates its superior cost-effectiveness and efficiency in industrial multi-metal wastewater remediation applications.

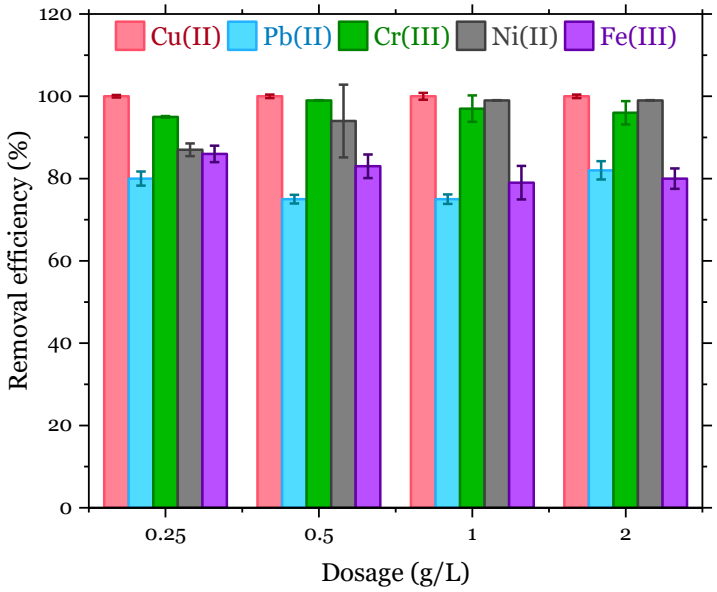

Figure 6 Removal of Cu(II) and Pb(II) from a multi-component system using CALF-20.

3.6 Fixed-bed dynamic breakthrough

A fixed bed dynamic breakthrough experiment was carried out to evaluate the competitive Cu(II) and Pb(II) adsorption on CALF-20. CALF-20 powder was packed in the fixed bed column where an eluant with 5.8 ppm Cu(II) and 4.0 ppm Pb(II) ion was applied[35]. During the experiment, the concentration of metal ions in the effluent was monitored by an ICP-OES instrument. The time that effluent first transverses the column and the first-time heavy metal ions were detected in the effluent were defined as the time zero and the breakthrough point, respectively. The concentration of detected points as a function of time was plotted in Figure 7 and the Thomas model[63] was applied for data fitting. As shown in Figure 7, Cu(II) has a breakthrough point of 380 minutes while Pb(II) starts to appear in the effluent at 30 minutes. The Thomas model, based

on the Langmuir isotherm model, was employed to characterize the breakthrough curves in fixed-bed columns,[63-64] facilitating the prediction of maximum adsorption capacities essential for treatment plant design. The high coefficients of determination (R^2) of Cu(II) (0.9540) and Pb(II) (0.9690) illustrated a good fit of the breakthrough data to the Thomas model, and more parameters of the fitting can be found in Table S7.

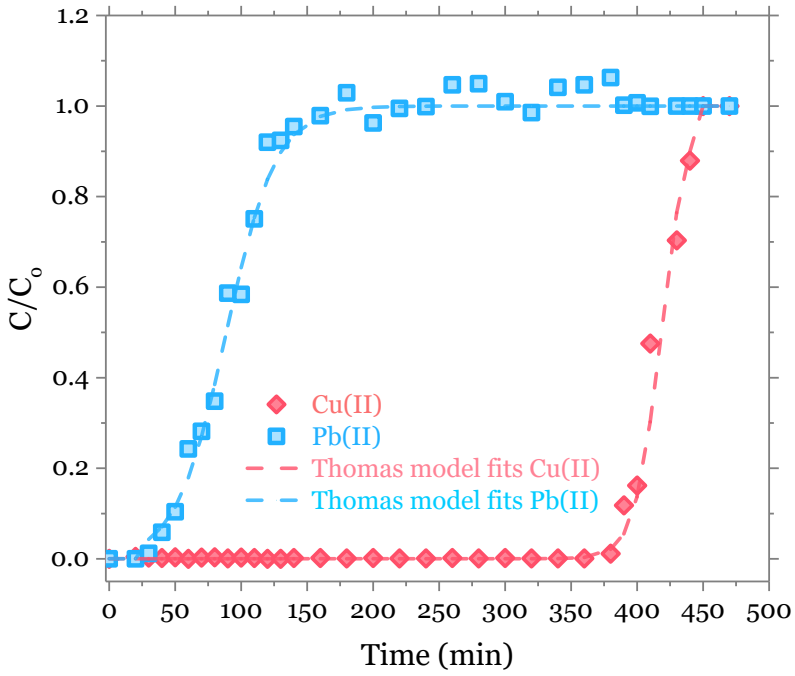

Figure 7 Breakthrough curve of Cu(II) and Pb(II) on a fixed-bed multi-component system.

4. CONCLUSION

This study presents the first comprehensive investigation into the use of CALF-20, a zinc-based MOF, for the efficient removal of Cu(II) and Pb(II) from aqueous solutions. Synthesized at room temperature using water and methanol as green solvents and low-cost, commercially available reagents, CALF-20 offers a highly cost-effective and scalable alternative to conventional MOF adsorbents. It demonstrated outstanding adsorption capacities of 250 mg/g for Cu(II) and 833

mg/g for Pb(II) at pH 5.3, respectively, outperforming many MOF adsorbents previously reported. Kinetic studies confirmed the pseudo-second-order behavior, while adsorption isotherm followed the Langmuir model. In a complex multi-ion environment, CALF-20 maintained good ability to remove multiple metal ions simultaneously, removing over 99% of Cu(II) and 82% of Pb(II), even at low dosages. Notably, the material retained over 90% of its capacity after five adsorption-desorption cycles, highlighting its long-term stability and reusability. The combined advantages of economic synthesis, industrial scalability, excellent adsorption performance, and regeneration capability position CALF-20 as a promising candidate for real-world industrial water treatment and environmental remediation.

ASSOCIATED CONTENT

Supporting Information. N_2 gas sorption, Zeta-potential, effect of pH, adsorption model fitting, kinetic model fitting, Cu(II) and Pb(II) removal efficiency, XPS survey spectrum, FTIR spectra, and SEM images of samples investigated are included in the Supporting Information section.

AUTHOR INFORMATION

Corresponding Author

*Corresponding author: Uttandaraman Sundararaj, ut@ucalgary.ca

Author Contributions

The manuscript was written through contributions of all authors. All authors have given approval to the final version of the manuscript.

Funding Sources

Funding from Natural Sciences and Engineering Research Council of Canada (NSERC) Discovery Grant 05503/2020 is highly appreciated.

Declaration of Competing Interest

The authors declare no competing financial interests.

Declaration of Generative AI and AI-Assisted Technologies in the Writing Process

During the preparation of this work the author(s) used ChatGPT to improve the readability and language of the manuscript. After using this tool/service, the authors reviewed and edited the content as needed and take full responsibility for the content of the published article.

458 REFERENCES

459 1. Wang, Z.; Luo, P.; Zha, X.; Xu, C.; Kang, S.; Zhou, M.; Nover, D.; Wang, Y., Overview
460 assessment of risk evaluation and treatment technologies for heavy metal pollution of water and
461 soil. *Journal of Cleaner Production* **2022,** *379*, 134043.
462 https://doi.org/10.1016/j.jclepro.2022.134043.

463 2. Bilal, M.; Shah, J. A.; Ashfaq, T.; Gardazi, S. M. H.; Tahir, A. A.; Pervez, A.; Haroon, H.;
464 Mahmood, Q., Waste biomass adsorbents for copper removal from industrial wastewater—A
465 review. *Journal of Hazardous Materials* **2013,** *263*, 322-333.
466 https://doi.org/10.1016/j.jhazmat.2013.07.071.

467 3. Kumar, V.; Dwivedi, S. K.; Oh, S., A critical review on lead removal from industrial
468 wastewater: Recent advances and future outlook. *Journal of Water Process Engineering* **2022,**
469 *45*, 102518. https://doi.org/10.1016/j.jwpe.2021.102518.

470 4. Wadhawan, S.; Jain, A.; Nayyar, J.; Mehta, S. K., Role of nanomaterials as adsorbents in
471 heavy metal ion removal from waste water: A review. *Journal of Water Process Engineering*
472 **2020,** *33*, 101038. https://doi.org/10.1016/j.jwpe.2019.101038.

473 5. Fu, F.; Wang, Q., Removal of heavy metal ions from wastewaters: A review. *Journal of*
474 *Environmental Management* **2011,** *92* (3), 407-418.
475 https://doi.org/10.1016/j.jenvman.2010.11.011.

476 6. Qasem, N. A. A.; Mohammed, R. H.; Lawal, D. U., Removal of heavy metal ions from
477 wastewater: a comprehensive and critical review. *npj Clean Water* **2021,** *4* (1), 36.
478 https://doi.org/10.1038/s41545-021-00127-0.

7. Satyam, S.; Patra, S., Innovations and challenges in adsorption-based wastewater remediation: A comprehensive review. *Heliyon* **2024,** *10* (9). https://doi.org/10.1016/j.heliyon.2024.e29573.

8. Zhou, H.-C.; Long, J. R.; Yaghi, O. M., Introduction to metal-organic frameworks. *Chemical Reviews* **2012,** *112* (2), 673-674. https://doi.org/10.1021/cr300014x.

9. Zhou, H.-C.; Kitagawa, S., Metal-organic frameworks (MOFs). *Chemical Society Reviews* **2014,** *43* (16), 5415-5418. https://doi.org/10.1039/c4cs90059f.

10. Lin, G.; Zeng, B.; Li, J.; Wang, Z.; Wang, S.; Hu, T.; Zhang, L., A systematic review of metal organic frameworks materials for heavy metal removal: Synthesis, applications and mechanism. *Chemical Engineering Journal* **2023,** *460*, 141710. https://doi.org/10.1016/j.cej.2023.141710.

11. Mane, P. V.; Rego, R. M.; Yap, P. L.; Losic, D.; Kurkuri, M. D., Unveiling cutting-edge advances in high surface area porous materials for the efficient removal of toxic metal ions from water. *Progress in Materials Science* **2024,** *146*, 101314. https://doi.org/10.1016/j.pmatsci.2024.101314.

12. Batten, S. R.; Champness, N. R.; Chen, X.-M.; Garcia-Martinez, J.; Kitagawa, S.; Öhrström, L.; O'Keeffe, M.; Paik Suh, M.; Reedijk, J., Terminology of metal-organic frameworks and coordination polymers (IUPAC recommendations 2013). *Pure and Applied Chemistry* **2013,** *85* (8). https://doi.org/10.1351/pac-rec-12-11-20.

13. O'Keeffe, M.; Peskov, M. A.; Ramsden, S. J.; Yaghi, O. M., The Reticular Chemistry Structure Resource (RCSR) Database of, and Symbols for, Crystal Nets. *Accounts of Chemical Research* **2008,** *41* (12), 1782-1789. https://doi.org/10.1021/ar800124u.

14. Yaghi, O. M., Reticular Chemistry—Construction, Properties, and Precision Reactions of Frameworks. *Journal of the American Chemical Society* **2016,** *138* (48), 15507-15509. https://doi.org/10.1021/jacs.6b11821.

15. Yaghi, O. M., Reticular Chemistry in All Dimensions. *ACS Central Science* **2019,** *5* (8), 1295-1300. https://doi.org/10.1021/acscentsci.9b00750.

16. Xu, W.; Tu, B.; Liu, Q.; Shu, Y.; Liang, C.-C.; Diercks, C. S.; Yaghi, O. M.; Zhang, Y.-B.; Deng, H.; Li, Q., Anisotropic reticular chemistry. *Nature Reviews Materials* **2020,** *5* (10), 764-779. https://doi.org/10.1038/s41578-020-0225-x.

17. Zheng, Z.; Rampal, N.; Inizan, T. J.; Borgs, C.; Chayes, J. T.; Yaghi, O. M., Large language models for reticular chemistry. *Nature Reviews Materials* **2025**. https://doi.org/10.1038/s41578-025-00772-8.

18. Zadehahmadi, F.; Eden, N. T.; Mahdavi, H.; Konstas, K.; Mardel, J. I.; Shaibani, M.; Banerjee, P. C.; Hill, M. R., Removal of metals from water using MOF-based composite adsorbents. *Environmental Science: Water Research & Technology* **2023,** *9* (5), 1305-1330. https://doi.org/10.1039/D2EW00941B.

19. Bakhtiari, N.; Azizian, S., Adsorption of copper ion from aqueous solution by nanoporous MOF-5: A kinetic and equilibrium study. *Journal of Molecular Liquids* **2015,** *206*, 114-118. https://doi.org/10.1016/j.molliq.2015.02.009.

20. Rahimi, E.; Mohaghegh, N., Removal of Toxic Metal Ions from Sungun Acid Rock Drainage Using Mordenite Zeolite, Graphene Nanosheets, and a Novel Metal–Organic

Framework. *Mine Water and the Environment* **2016,** *35* (1), 18-28. https://doi.org/10.1007/s10230-015-0327-7.

21. David Shooto, N.; Dixon Dikio, E., Highly Porous MOF Adsorbent for Wastewater Treatment. *Asian Journal of Chemistry* **2018,** *30* (8), 1723-1730. https://doi.org/10.14233/ajchem.2018.21275.

22. Ghaedi, A. M.; Panahimehr, M.; Nejad, A. R. S.; Hosseini, S. J.; Vafaei, A.; Baneshi, M. M., Factorial experimental design for the optimization of highly selective adsorption removal of lead and copper ions using metal organic framework MOF-2 (Cd). *Journal of Molecular Liquids* **2018,** *272*, 15-26. https://doi.org/10.1016/j.molliq.2018.09.051.

23. Zhou, L.; Li, N.; Owens, G.; Chen, Z., Simultaneous removal of mixed contaminants, copper and norfloxacin, from aqueous solution by ZIF-8. *Chemical Engineering Journal* **2019,** *362*, 628-637. https://doi.org/10.1016/j.cej.2019.01.068.

24. Guo, Y.; Jia, Z.; Shi, Q.; Liu, Z.; Wang, X.; Li, L., Zr (IV)-based coordination porous materials for adsorption of Copper(II) from water. *Microporous and Mesoporous Materials* **2019,** *285*, 215-222. https://doi.org/10.1016/j.micromeso.2019.05.020.

25. Ahmadijokani, F.; Tajahmadi, S.; Bahi, A.; Molavi, H.; Rezakazemi, M.; Ko, F.; Aminabhavi, T. M.; Arjmand, M., Ethylenediamine-functionalized Zr-based MOF for efficient removal of heavy metal ions from water. *Chemosphere* **2021,** *264*, 128466. https://doi.org/10.1016/j.chemosphere.2020.128466.

26. Morcos, G. S.; Ibrahim, A. A.; El-Sayed, M. M. H.; El-Shall, M. S., High performance functionalized UiO metal organic frameworks for the efficient and selective adsorption of Pb (II)

ions in concentrated multi-ion systems. *Journal of Environmental Chemical Engineering* **2021,** *9* (3), 105191. https://doi.org/10.1016/j.jece.2021.105191.

27. Zheng, T.-T.; Zhao, J.; Fang, Z.-W.; Li, M.-T.; Sun, C.-Y.; Li, X.; Wang, X.-L.; Su, Z.-M., A luminescent metal organic framework with high sensitivity for detecting and removing copper ions from simulated biological fluids. *Dalton Transactions* **2017,** *46* (8), 2456-2461. https://doi.org/10.1039/C6DT04630D.

28. Shah, S. S. A.; Sohail, M.; Murtza, G.; Waseem, A.; Rehman, A. u.; Hussain, I.; Bashir, M. S.; Alarfaji, S. S.; Hassan, A. M.; Nazir, M. A.; Javed, M. S.; Najam, T., Recent trends in wastewater treatment by using metal-organic frameworks (MOFs) and their composites: A critical view-point. *Chemosphere* **2024,** *349*, 140729. https://doi.org/10.1016/j.chemosphere.2023.140729.

29. Severino, M. I.; Gkaniatsou, E.; Nouar, F.; Pinto, M. L.; Serre, C., MOFs industrialization: a complete assessment of production costs. *Faraday Discussions* **2021,** *231* (0), 326-341. https://doi.org/10.1039/D1FD00018G.

30. Lin, J.-B.; Nguyen, T. T. T.; Vaidhyanathan, R.; Burner, J.; Taylor, J. M.; Durekova, H.; Akhtar, F.; Mah, R. K.; Ghaffari-Nik, O.; Marx, S.; Fylstra, N.; Iremonger, S. S.; Dawson, K. W.; Sarkar, P.; Hovington, P.; Rajendran, A.; Woo, T. K.; Shimizu, G. K. H., A scalable metal-organic framework as a durable physisorbent for carbon dioxide capture. *Science* **2021,** *374* (6574), 1464-1469. https://doi.org/10.1126/science.abi7281.

31. Drwęska, J.; Roztocki, K.; Janiak, A., Advances in Chemistry of CALF-20, a Metal-Organic Framework for Industrial Gas Applications. *Chemical Communications* **2025**. https://doi.org/10.1039/D4CC05744A.

32. Chakraborty, D.; Yurdusen, A.; Mouchaham, G.; Nouar, F.; Serre, C., Large-Scale Production of Metal–Organic Frameworks. *Advanced Functional Materials* **2024,** *34* (43), 2309089. https://doi.org/10.1002/adfm.202309089.

33. Deng, Z.; Yang, L.; Xiong, H.; Liu, J.; Liu, X.; Zhou, Z.; Chen, S.; Wang, Y.; Wang, H.; Chen, J.; Deng, S.; Chen, B.; Wang, J., Green and Scalable Preparation of an Isomeric CALF-20 Adsorbent with Tailored Pore Size for Molecular Sieving of Propylene from Propane. *Small Methods* **2024**, 2400838. https://doi.org/10.1002/smtd.202400838.

34. Higuchi, Y.; Sugita, M.; Moriya, S.; Takewaki, T.; Tanaka, S., Rapid synthesis of metal-organic framework CALF-20 in H2O/methanol solution under room temperature and normal pressure. *Microporous and Mesoporous Materials* **2024,** *374*, 113137. https://doi.org/10.1016/j.micromeso.2024.113137.

35. Bi, G.; Li, X.; Du, X.; Sun, X.; Yao, W., Remediation of heavy metal pollution from coal mine effluent using metal-organic frameworks (MOF): Impact of water media, operational factors and metal characteristics. *Minerals* **2024,** *14* (8), 764. https://doi.org/10.3390/min14080764.

36. Zhai, Q.-G.; Lu, C.-Z.; Wu, X.-Y.; Batten, S. R., Coligand Modulated Six-, Eight-, and Ten-Connected Zn/Cd-1,2,4-Triazolate Frameworks Based on Mono-, Bi-, Tri-, Penta-, and

Heptanuclear Cluster Units. *Crystal Growth & Design* **2007,** *7* (11), 2332-2342. https://doi.org/10.1021/cg070593q.

37. Wei, X.-F.; Miao, J.; Shi, L.-L., Synthesis, Crystal Structure, and Luminescent Property of One 3D Porous Metal-Organic Framework With dmc Topology. *Synthesis and Reactivity in Inorganic, Metal-Organic, and Nano-Metal Chemistry* **2014,** *46* (3), 365-369. https://doi.org/10.1080/15533174.2014.988251.

38. Corella-Ochoa, M. N.; Benet-Buchholz, J.; Martínez-Belmonte, M.; Galán-Mascarós, J. R., Spontaneous Magnetization in Homometallic μ6-Oxalate Coordination Polymers. *Inorganic Chemistry* **2015,** *54* (10), 4678-4687. https://doi.org/10.1021/ic503032g.

39. Chen, Z.; Ho, C.-H.; Wang, X.; Vornholt, S. M.; Rayder, T. M.; Islamoglu, T.; Farha, O. K.; Paesani, F.; Chapman, K. W., Humidity-Responsive Polymorphism in CALF-20: A Resilient MOF Physisorbent for CO2 Capture. *ACS Materials Letters* **2023,** *5* (11), 2942-2947. https://doi.org/10.1021/acsmaterialslett.3c00930.

40. Thommes, M.; Kaneko, K.; Neimark, A. V.; Olivier, J. P.; Rodriguez-Reinoso, F.; Rouquerol, J.; Sing, K. S. W., Physisorption of gases, with special reference to the evaluation of surface area and pore size distribution (IUPAC Technical Report). *Pure and Applied Chemistry* **2015,** *87* (9-10), 1051-1069. https://doi.org/10.1515/pac-2014-1117.

41. Jagiello, J.; Olivier, J. P., 2D-NLDFT adsorption models for carbon slit-shaped pores with surface energetical heterogeneity and geometrical corrugation. *Carbon* **2013,** *55*, 70-80. https://doi.org/10.1016/j.carbon.2012.12.011.

42. Sutton, A. L.; Sadiq, M. M.; Mardel, J. I.; Hill, M. R., Hydrogen storage of commercially scalable CALF-20: a study at cryogenic and near-ambient temperatures. *CrystEngComm* **2024,** *26* (42), 6003-6007. https://doi.org/10.1039/D4CE00861H.

43. Wang, H.; Wang, S.; Wang, S.; Fu, L.; Zhang, L., The one-step synthesis of a novel metal–organic frameworks for efficient and selective removal of Cr(VI) and Pb(II) from wastewater: Kinetics, thermodynamics and adsorption mechanisms. *Journal of Colloid and Interface Science* **2023,** *640*, 230-245. https://doi.org/10.1016/j.jcis.2023.02.108.

44. Hoseinian, F. S.; Ramshini, S.; Rezai, B.; Kowsari, E.; Safari, M., Toxic heavy metal ions removal from wastewater by ion flotation using a nano collector. *Minerals Engineering* **2023,** *204*, 108380. https://doi.org/10.1016/j.mineng.2023.108380.

45. Corbett, J. F., Pseudo first-order kinetics. *Journal of Chemical Education* **1972,** *49* (10), 663. https://doi.org/10.1021/ed049p663.

46. Ho, Y.-S.; McKay, G., Pseudo-second order model for sorption processes. *Process Biochemistry* **1999,** *34* (5), 451-465. https://doi.org/10.1016/S0032-9592(98)00112-5.

47. Aharoni, C.; Tompkins, F., Kinetics of adsorption and desorption and the Elovich equation. In *Advances in Catalysis*, Elsevier: 1970; Vol. 21, pp 1-49. https://doi.org/10.1016/S0360-0564(08)60563-5.

48. Weber, W. J.; Morris, J. C., Kinetics of adsorption on carbon from solution. *Journal of the Sanitary Engineering Division* **1963,** *89* (2), 31-59. https://doi.org/10.1061/JSEDAI.0000430.

49. Wang, J.; Xu, L.; Meng, Y.; Cheng, C.; Li, A., Adsorption of Cu2+ on new hyper-crosslinked polystyrene adsorbent: Batch and column studies. *Chemical Engineering Journal* **2011,** *178*, 108-114. https://doi.org/10.1016/j.cej.2011.10.022.

50. Ghorbani, M.; Nowee, S. M.; Ramezanian, N.; Raji, F., A new nanostructured material amino functionalized mesoporous silica synthesized via co-condensation method for Pb(II) and Ni(II) ion sorption from aqueous solution. *Hydrometallurgy* **2016,** *161*, 117-126. https://doi.org/10.1016/j.hydromet.2016.02.002.

51. Kobielska, P. A.; Howarth, A. J.; Farha, O. K.; Nayak, S., Metal–organic frameworks for heavy metal removal from water. *Coordination Chemistry Reviews* **2018,** *358*, 92-107. https://doi.org/10.1016/j.ccr.2017.12.010.

52. Langmuir, I., The constitution and fundamental properties of solids and liquids. Part I. Solids. *Journal of the American Chemical Society* **1916,** *38* (11), 2221-2295. https://doi.org/10.1021/ja02268a002.

53. Freundlich, H., Über die adsorption in lösungen. *Zeitschrift für physikalische Chemie* **1907,** *57* (1), 385-470. https://doi.org/10.1515/zpch-1907-5723.

54. Sips, R., On the structure of a catalyst surface. *The Journal of Chemical Physics* **1948,** *16* (5), 490-495. https://doi.org/10.1063/1.1746922.

55. Temkin, M., Kinetics of ammonia synthesis on promoted iron catalysts. *Acta Physiochim. URSS* **1940,** *12*, 327-356.

638 56. Bui, N. T.; Kang, H.; Teat, S. J.; Su, G. M.; Pao, C.-W.; Liu, Y.-S.; Zaia, E. W.; Guo, J.;
639 Chen, J.-L.; Meihaus, K. R.; Dun, C.; Mattox, T. M.; Long, J. R.; Fiske, P.; Kostecki, R.; Urban,
640 J. J., A nature-inspired hydrogen-bonded supramolecular complex for selective copper ion
641 removal from water. *Nature Communications* **2020,** *11* (1), 3947. https://doi.org/10.1038/s41467-
642 020-17757-6.

643 57. Cai, H.; Sun, Y.; Zhang, X.; Zhang, L.; Liu, H.; Li, Q.; Bo, T.; Zhou, D.; Wang, C.; Lian, J.,
644 Reduction Temperature-Dependent Nanoscale Morphological Transformation and Electrical
645 Conductivity of Silicate Glass Microchannel Plate. *Materials* **2019,** *12* (7), 1183.
646 https://doi.org/10.3390/ma12071183.

647 58. Bagus, P. S.; Nelin, C. J.; Brundle, C. R., Chemical significance of x-ray photoelectron
648 spectroscopy binding energy shifts: A Perspective. *Journal of Vacuum Science & Technology A*
649 **2023,** *41* (6). https://doi.org/10.1116/6.0003081.

650 59. Paynter, R., XPS theory. *INRS-Énergie, Matériaux et Télécommunications, Quebec.*
651 *http://saturno. fmc. uam. es/web/solidoII/propiedades_de_transporte/XPS_Paynter_t. pdf* **2000**.

652 60. Zhu, C.; Hou, J.; Wang, X.; Wang, S.; Xu, H.; Hu, J.; Jing, L.; Wang, S., Optimizing ligand-
653 to-metal charge transfer in metal–organic frameworks to enhance photocatalytic performance.
654 *Chemical Engineering Journal* **2024,** *499*, 156527. https://doi.org/10.1016/j.cej.2024.156527.

655 61. Xu, Y.; Huang, Y.; Xie, Y.; Chen, X., Efficient and Rapid Extraction of Gold from E-Waste
656 via Tailoring the Skeleton Environment of Covalent Organic Framework. *ACS Applied Materials*
657 *& Interfaces* **2025,** *17* (8), 12317-12327. https://doi.org/10.1021/acsami.4c22268.

62. Jasi, A. BASF commercially produces metal-organic frameworks for CO2 capture in world first. https://www.thechemicalengineer.com/news/basf-commercially-produces-metal-organic-frameworks-for-co2-capture-in-world-first/.

63. Thomas, H. C., Heterogeneous ion exchange in a flowing system. *Journal of the American Chemical Society* **1944,** *66* (10), 1664-1666. https://doi.org/10.1021/ja01238a017.

64. Mao, J.; Lin, S.; Lu, X. J.; Wu, X. H.; Zhou, T.; Yun, Y.-S., Ion-imprinted chitosan fiber for recovery of Pd(II): Obtaining high selectivity through selective adsorption and two-step desorption. *Environmental Research* **2020,** *182*, 108995. https://doi.org/10.1016/j.envres.2019.108995.

669 For Table of Contents only

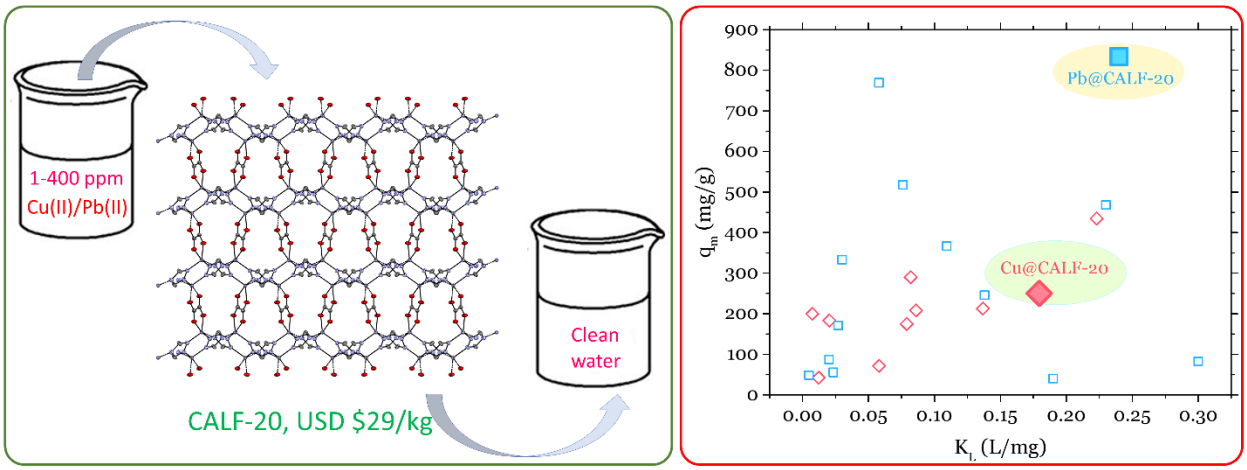

670